ELECTRICAL STIMULATION FOR PAIN SUPPRESSION: MATHEMATICAL AND PHYSICAL MODELS

A Thesis

Presented to the Faculty of the Graduate School

of Cornell University

In Partial Fulfillment of the Requirements for the Degree of

Master of Engineering

by

Francis Marion Moore

May 2007

ABSTRACT

Finite element models of increasing complexity were generated in the ANSYS finite element modeling program to determine the electric field and current properties in the body as a result of the transcutaneous electric nerve stimulation (TENS) device. The initial models consist of one-, two-, and three-layer structures, and the final model was a 7,415 node two-dimensional model of the human arm. To validate the ANSYS calculations, one-, two-, and three-layer phantom models were developed using agar, deionized (DI) water, and sodium chloride in varying concentrations. A summing amplifier was built to combine multiple stimulating waveforms at different frequencies from two function generators at two frequencies F_1 and F_2. Current measurements from the phantom models were compared to ANSYS calculations on corresponding finite element models. The ANSYS program was validated for modeling of single-layer models. Multiple layers of gels of different resistivity exhibited ion leaching problems which made them unsuitable as phantom models. It is necessary, therefore, to develop and validate an alternative phantom model for modeling electric field and current properties of multi-layer systems.

A technique was developed for transforming cross-sectional images of body parts into mesh diagrams suitable use in ANSYS. Body images from "The Visible Human Project" were taken and processed such that eight different tissue types and their location could be identified. Electrical properties were determined for muscle, skin, fat, cortical and cancellous bone, blood, connective tissue, and nervous tissue for use in the ANSYS simulation models. A cross-section of a male arm was processed and analyzed.

BIOGRAPHICAL SKETCH

Francis entered Cornell as a freshman in 2001, spent one semester at SUNY Stony Brook in 2003, and returned to Cornell where in 2005 he received his Bachelor of Science in Biological Engineering. He attended the Cornell graduate school a year later and completed his Master of Engineering in Biological Engineering in 2007.

To Bernard Cecil Moore & Marianne Lorraine Spatz

ACKNOWLEDGMENTS

Thanks to Dr. Ron Gorewit and Dr. Dan Aneshansley for putting up with me and the constant software difficulties which arose throughout this project. Without their help, the phantom model designs could never have been completed, and I am grateful for their input on this project.

Many thanks to Andrew Hocking of Kionix in Ithaca, NY and to Adam Fox of Sikorski in New Haven, CT. Andrew's advice on ANSYS modeling and Adam's support throughout the entire course of my graduate program have been priceless, and I cannot thank these two enough for their help over the last year.

Thanks to my family back home for listening to me complain on the phone when frustrated, for offering problem-solving advice, and for being supportive for long enough for me to get through graduate school in the first place.

TABLE OF CONTENTS

LIST OF FIGURES

LIST OF TABLES

LIST OF ABBREVIATIONS

ANSYS	Finite element modeling software used for this project
FEM	Finite Element Model (Modeling)
Hz	Hertz
Osm	Osmole(s)
RMS	Root Mean Square
TENS	Transcutaneous Electric Nerve Stimulation

LIST OF SYMBOLS

A	Amperes (When used as a unit)
A	Area (When used as a variable)
d	Distance between capacitor plates
dF	Frequency Difference (Pulse Waveform)
DI	Deionized (In reference to water)
$F_{\#}$	Frequency (Generator designated by #)
G	Gain
I	Current
L	Depth of gel
r	Radius
R	Resistance
V	Volts
Vgel	Voltage across the gel
Vsys	Voltage across the resistor and gel in series
ε	Permittivity (Capacitance)
ρ	Resistivity
Ω	Ohms (Units of Resistance)
M Ω	Megaohms

CHAPTER 1

ELECTRICAL NERVE STIMULATION

1.1 Introduction

Transcutaneous electrical nerve stimulation (TENS) is a pain relief procedure during which a low amplitude and frequency alternating electric current is passed between two electrodes across an affected body segment. The current passes through the pained body segment, stimulates contained nervous tissue, and results in an analgesic effect for the afflicted user. A typical battery operated TENS unit consists of a pulse generator, transformer, and frequency and intensity controls. TENS treatment is primarily used for chronic (non-acute) pain relief, often in post-surgical rehabilitation for back injuries (Yokoyama et. al, 2004), joint and knee injuries, and severe arthritis.

There are two primary and related theories for explaining the efficacy of TENS in chronic or acute pain relief. The gate theory (Wall, 1965) proposes that pain transmission relies on a 'gate' to the thalamus and cortex for nocireceptive information to be interpreted as pain. This theory postulates that inhibition of nocireceptors can be caused by rapid impulse activation of myelinated nerve fibers. The second related theory postulates that neurotransmitter exhaustion can be caused by rapid nerve activation outside of its refractory period, and that the temporary exhaustion of neurotransmitters would provide pain relief until such time as neurotransmitter synthesis had 'refilled' the synaptic junctions (Kaye, 2007).

1.2 TENS Devices

TENS devices typically use a low amplitude current at 80-100 Hz, potentially decreasing to 0-1.5 Hz at high intensity settings (Kaye, 2007). A TENS device was

designed which combines two alternating voltages at different frequencies, F_1 and F_2 (Hz) respectively. The current is applied between two electrodes and results in an altering electric field with a beat frequency of dF inside a body segment. In order to better understand how these electrical voltages and the currents they produce behave in body tissue, a finite element model and phantom models to verify the FEM modes were developed.

Visualization of the waveforms generated reveals a waveform which is produced by constructive and destructive interference and is cyclic every 1/dF seconds as shown in Appendix 1. The summation wave form, which visualizes the total system wave effect, is shown in Appendix 2. This is the resulting waveform which will be generated by the two signals, assuming both start in phase and have the same peak-to-peak amplitude. A phase shift would move the zero-voltage points on the X axis and the duration of the pulse, while the shape of the pulse would be altered by a variation in the amplitudes.

1.3 TENS Simulation

In order to simulate TENS treatment, a series of finite element models were created using ANSYS software on a Windows-based personal computer. The preliminary simplified models were created using ANSYS Educational 10, and the final model was created using ANSYS University 10. ANSYS software packages are available through ANSYS Inc.

To obtain properties necessary to simulate electrical conditions in a given body segment, a literature review identifying material properties (conductivity and permittivity) for eight biological tissues was performed. Material properties were determined for muscle, skin, fat, cortical and cancellous bone, blood, connective tissue, and nervous tissue. These values are noted in tables 1 and 2.

4,000 Hz	*Skin*	*Fat*	*Cortical Bone*	*Cancellous Bone*	*Blood*	*Connective Tissue*	*Nervous Tissue*	*Muscle*
Permittivity	1134.8	3876.2	995.5	3655.5	5255	23516	53401	68157
Conductivity	0.0002	0.023	0.020	0.082	0.700	0.386	0.033	0.335

Table 1 – Biomaterial Electrical Properties at 4,000 Hz Current (Gabriel, 1996)

4,122 Hz	*Skin*	*Fat*	*Cortical Bone*	*Cancellous Bone*	*Blood*	*Connective Tissue*	*Nervous Tissue*	*Muscle*
Permittivity	1134.8	3712.5	972.69	3557.1	5254.9	22319	52917	65717
Conductivity	0.0002	0.024	0.020	0.082	0.700	0.386	0.033	0.335

Table 2 – Biomaterial Electrical Properties at 4,122 Hz Current (Gabriel, 1996)

ANSYS electrical models use resistivity, which is the inverse of the conductivity, in order to determine the electrical conduction effects of the system (equation 1). Permittivity is used to determine capacitative effects of the system (equation 2). The electrical resistance of a tissue is related to the resistivity and the physical dimensions as shown in equation 3. These equations assume cylindrical volumes.

$$\rho = \frac{1}{\sigma} \qquad (1)$$

$$C = \varepsilon \cdot \frac{\pi \cdot r^2}{d} \qquad (2)$$

$$R = \rho \cdot \frac{\pi \cdot r^2}{l} \qquad (3)$$

In order to use the material values shown in tables 1 and 2, several assumptions were made. It was assumed that each tissue is homogeneous in nature, allowing for no variation of resistivity or permittivity within a given type of layer. Each layer was assumed to bear the same material properties regardless of its electrical field

orientation.

Calculations made in the finite element model on the basis of the resistivity and conductivity of each tissue type supply the current density (current per unit area), the electric potential, and the electric field. Calculations for the electric potential and current were performed by manipulation of Ohm's Law (equation 4) in discretized form. Current density was calculated as shown in equation 5, while the electric field was determined in a discretized finite element model by the method shown in equation 6.

$$V = I \cdot R \qquad (4)$$

$$J = \sigma \cdot \mathrm{E} \qquad (5)$$

$$\vec{E} = -\nabla V \qquad (6)$$

Calculation of total current in the finite element model can be performed by summation of unitized current densities over all inputs or outputs of the system, as shown in equation 7.

$$I = \left(\sum J \cdot dA\right)_{in} \text{ or } I = \left(\sum J \cdot dA\right)_{out} \qquad (7)$$

CHAPTER 2

COMPUTER SIMULATION OF ELECTRICAL PROPERTIES

2.1 Simple Simulation Models of One to Three Layers

Three two-dimensional finite element models were generated during the course of this project: one-, two-, and three-layer simplified models. All three models were created and generated in ANSYS.

The simplified models were generated using limited 2D rectangular geometry as shown in figure 1 in order to easily validate finite element (FE) calculations against phantom models. The simplified geometry allowed for creation of inexpensive agar and sodium chloride gel phantom models of known geometry and electrical characteristics that could be analyzed using the ANSYS simulation process.

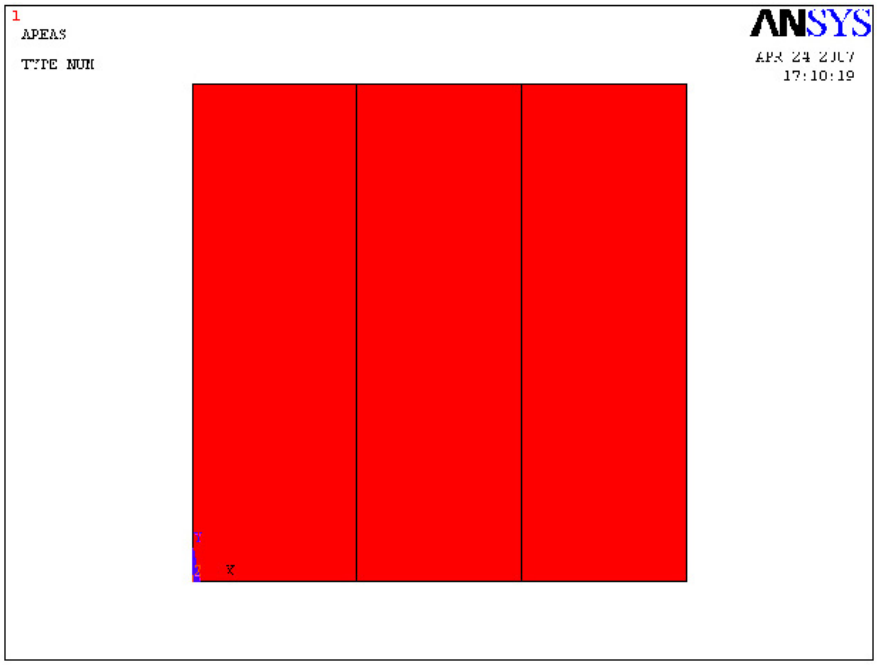

Figure 1 – Three-Layer Model Geometry

The one-layer model contained a single homogeneous layer. The resistivity of the layer was set equal to that of the phantom model used in each validation check, as explained in section 3.4. The two-layer model contained two homogeneous layers of

different resistivities in order to determine if finite element calculations can be validated between different layer types. The resistivities for the two-layer model corresponded to those found experimentally for gels with 135 and 435 mOsm (milliosmole) salt concentrations. The three-layer model contained two types of homogeneous layer arranged sequentially with resistivities that match a phantom model comprised of a 0, 290, and 0 mOsm salt concentration in sequence, respectively. This was used as a model of highly conductive tissue (muscle or other internal tissues) surrounded by a less conductive one (skin).

Each ANSYS simulation model was created using the same general procedure. First, a series of keypoints defining line intersections were numerically assigned in the active plane (X,Y). The keypoints were generated by defining coordinate locations in the (X,Y) plane. These points were not necessary for models containing only rectangular geometry, but were used in order to maintain consistency because they were necessary for generation of the more complex model.

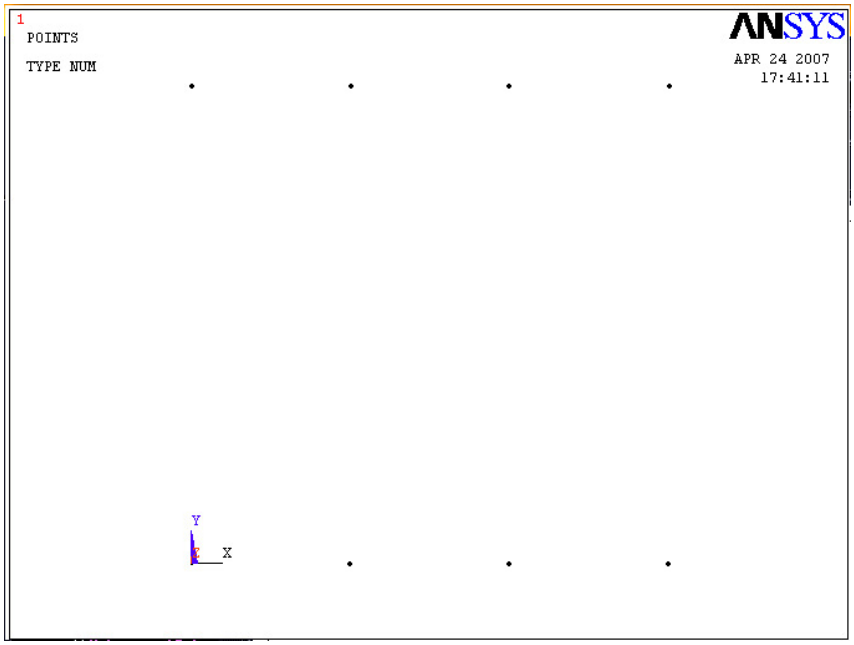

Figure 2 – Keypoints for Three-Layer Model

Following keypoint generation, lines were manually placed connecting sequential keypoints to each other to denote the boundaries of each layer in the model. Areas are defined by sections of space encompassed by connected lines. Areas are defined in ANSYS by selecting the lines bordering the space intended for the area. The areas defined the material bodies of each tissue once they were meshed (discretized). The lines and areas for the three-layer model are shown in figure 3.

Once areas were defined, the ANSYS *GLUE* command was used on each area in order to link each tissue into one solid structure. If the areas were not glued together, each would act as an isolated structure with perfect insulation from its neighboring tissues. The *GLUE* command set their boundaries to being in contact with each other and allows for conductive transfer between internal connections.

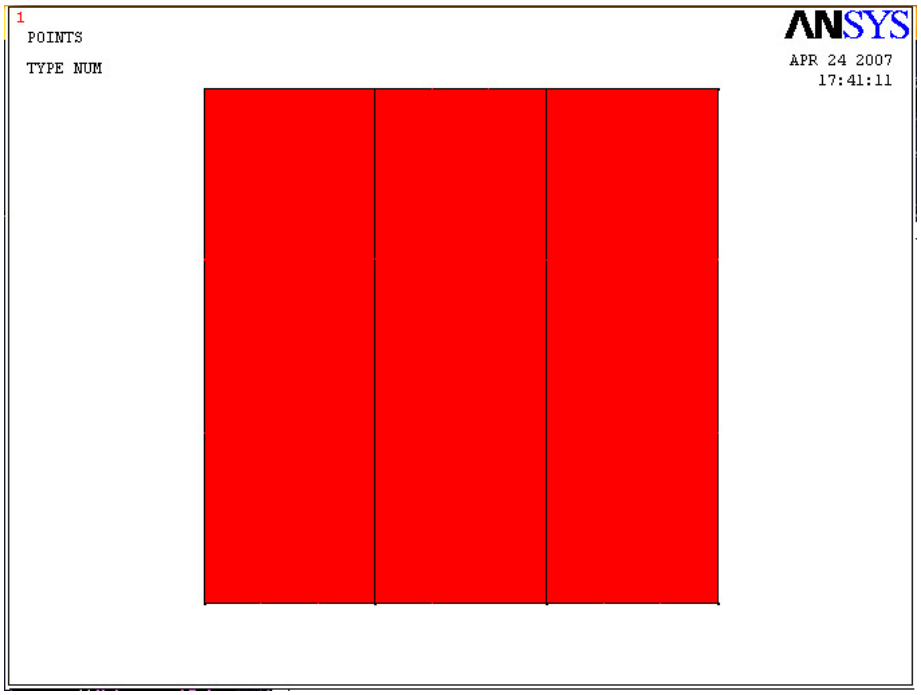

Figure 3 – Lines and Areas for Three-Layer Model

The model was meshed next in order to discretize the tissues into a matrix of resistivity, permittivity, and coordinate location values. This is the finite element procedure, and each mesh intersection (called a node) is a point where the system will

calculate differences in electrical properties relative to surrounding nodes. Mesh density is chosen by selecting a meshing level in ANSYS, and higher levels will produce a greater number of nodes for calculation. ANSYS automatically adjusts mesh density to increase the number of nodes in small areas and near lines. The physical resolution of the simulation is determined by mesh size. Meshes will either be based on quadrilateral geometry (as shown in figure 4) or on triangular geometry. The only difference between these is the method used to optimize the meshing. Triangular meshes are better for complex geometry, while quadrilateral meshes are better suited for rectangular geometry. If the electrical properties change significantly within a small area of the model, finer meshing is necessary or information will be lost. This is the equivalent of picking an appropriate sampling rate for data acquisition, where picking too low a sampling rate may exclude important frequency information. An example of quadrilateral meshing is shown in figure 4.

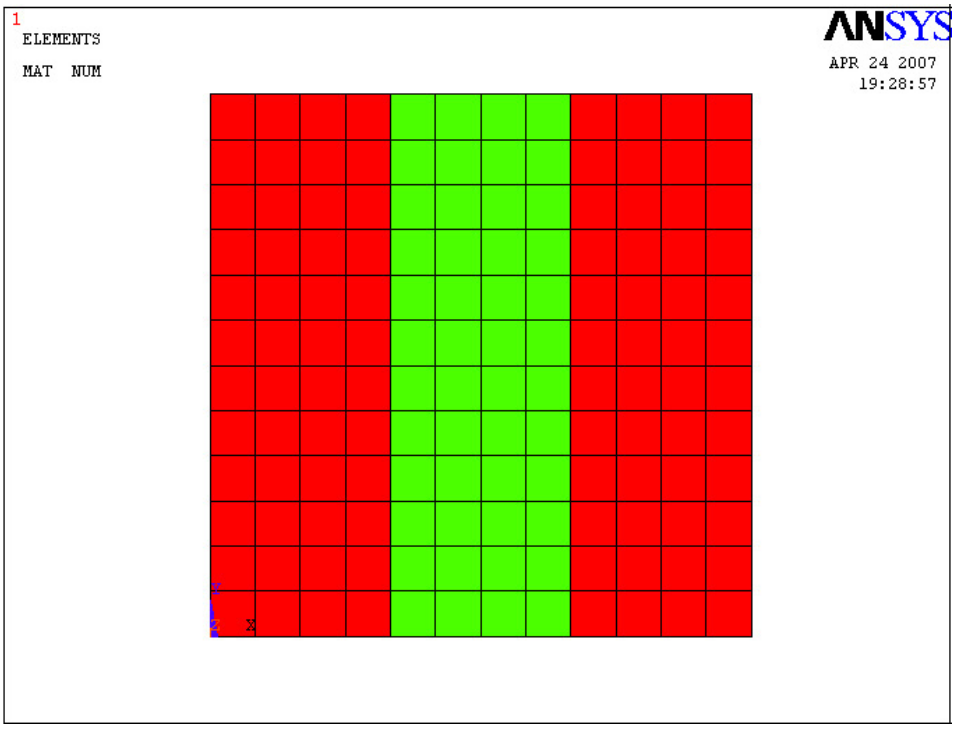

Figure 4- Mesh Structure for Three-Layer Model

The final step prior to calculation is to set up the conditions of the model. The alternating current is applied to the model by designating root mean square voltages on the left and right edges of the model. The left edge will be assigned the voltage applied to this side relative to the right side of the gel. This corresponds to the input voltage across the gel in the phantom model. Next, initial conditions are set on the model placing the internal voltage at 0.000 volts, which would designate an initially uncharged state for the tissues. Finally, the analysis is set to a harmonic analysis, and the frequency is set to F1 hertz. Calculations of current density, electric field, and electric potential were now calculated for each model.

2.2 Visualization of Results

On completion of model analysis, results were available in nodal listing form or in visual format. The simulation results were as follows for each finite element model.

The one-layer simplified model showed no variation vertically as this was effectively a one-dimensional model due to vertical homogeneity of its electrical properties. Given the geometry simplified this model to a one-dimensional calculation, the same amount of current was be seen at the left and right edges of the model, which demonstrated current continuity. Finally, it had a constant-rate potential drop across its entirety, which matched expectations because there was only one material type in this model. As a result of the constant-rate potential drop, it also featured a uniform electric field. All expectations were qualitatively met in the one-layer simplified model.

The two-layer simplified model (145 and 435 mOsm layers) featured an electric potential drop that was greater in the higher resistivity 145 mOsm layer than it was in the 435 mOsm layer. This also indicated a higher magnitude electric field in

the 145 mOsm tissue than in the 435 mOsm layer. Due to the geometry of the model, no y-axis variation in any electrical properties was seen. Finally, left-edge current equaled the right-edge current. Qualitatively, the two-layer simplified model met our calculative expectations.

The three-layer simplified model with resistivities corresponding to 0 mOsm, 290 mOsm and 0 mOsm salt respectively showed many of the same features as the two-layer model. There was no variation vertically as this was also effectively a one-dimensional model. There was a greater potential drop across the first and third layers because of their higher resistivities. The electric field calculations were performed using equation 6 from chapter 1. Given the electric field was proportional to the voltage change, a higher amplitude electric field in the first and third layers due to the higher potentials was expected. Additionally, as the voltage did not vary along the y-axis, a vector analysis of the electric field did not yield any vertical electric field components. The three-layer model qualitatively matched our expectations for the system.

Figures 5-7 show the electric potential, electric field, and current density respectively for the one-, two-, and three-layer models. MX and MN indicate the locations maximum and minimum values in the graph. The contour colors indicate the voltage relative to the grounded right side of each model. As all qualitative expectations were met, quantitative validation was then performed in order to determine numerical accuracy of our simulations.

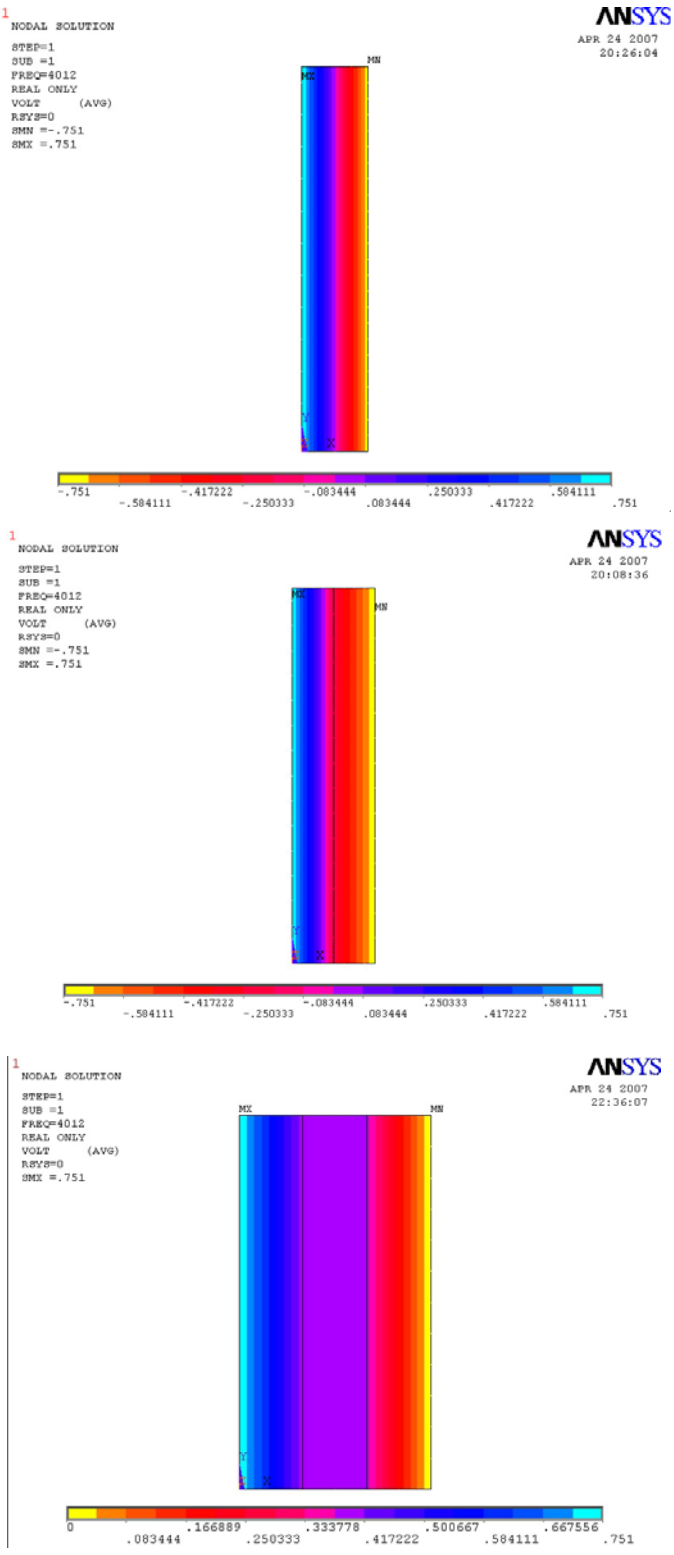

Figure 5 - Electric Potential (V) for 1, 2, and 3-Layer Models (MN, MX denote minima and maxima)

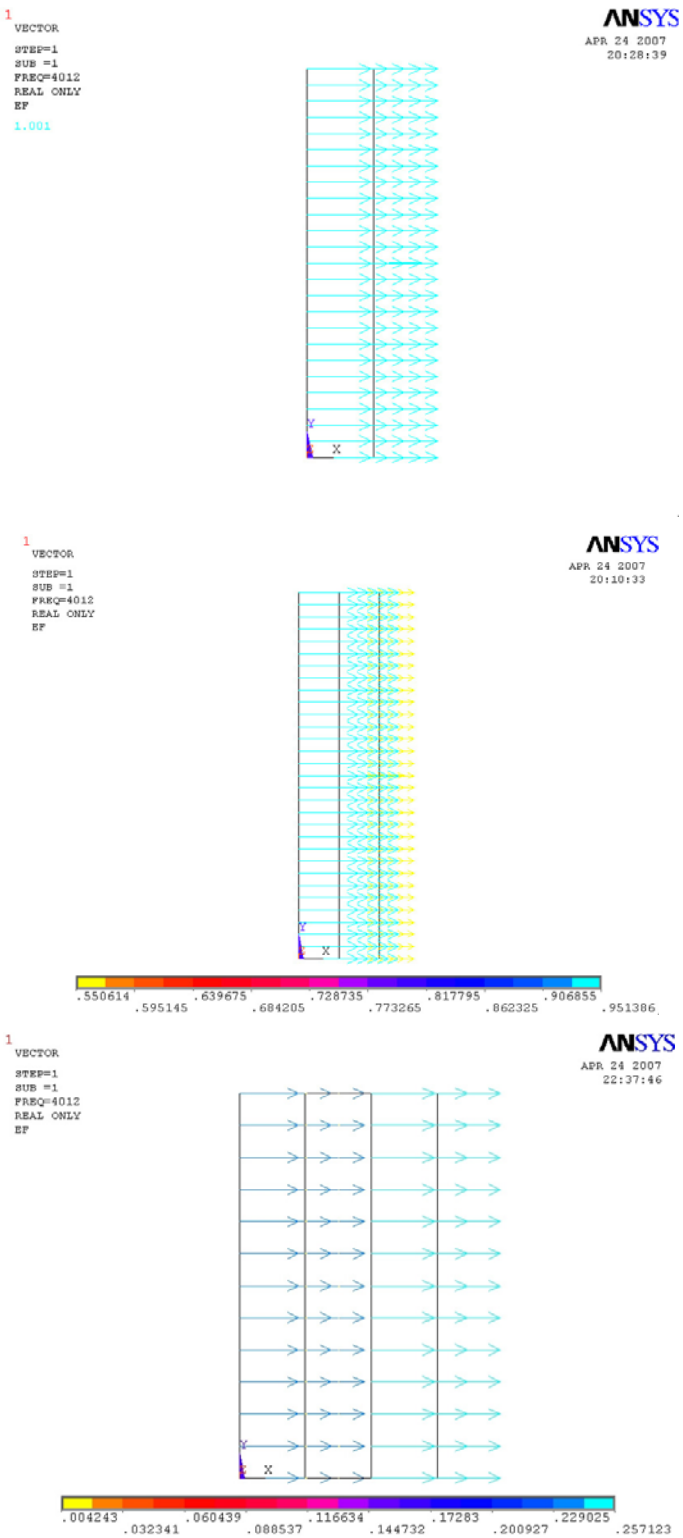

Figure 6 – Electric Field (V/m) for 1, 2, and 3-Layer Models

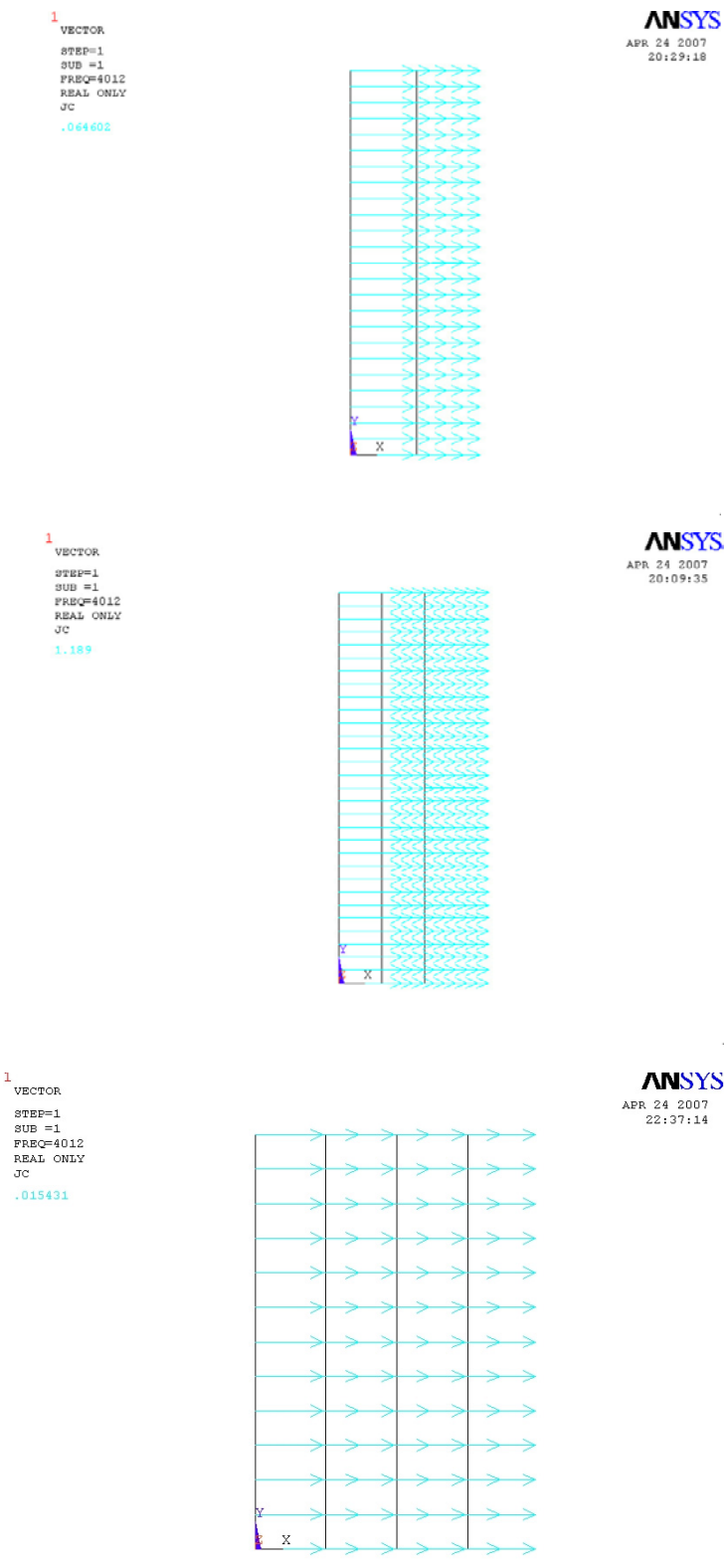

Figure 7 – Current Density (A/m^2) for 1, 2, and 3-Layer Models

CHAPTER 3

VALIDATION OF THE ANSYS SIMULATION

3.1 Validation Methodology

A validation procedure was needed to determine if the finite element modeling method is a valid means of modeling the electrical properties of the human body and the electrical state as a result of specific stimulation. To this end, phantom models were produced from agar gel, deionized water, and varying concentrations of sodium chloride. A simple summing amplifier was used to combine two voltage sources of different frequencies. A know resister was placed in series with gels which were placed between two stainless steel electrodes. The current through the gel and voltage drop across the gel was determined and the resistance of the gel calculated. The resistivity of the gel could then be calculated from its resistance and physical dimensions with the assumption of homogeneous concentration.

The resistivities of the simple models described in chapter 3 were set equal to the resistivities calculated for the gels, and the simulated current values were compared to the experimental values calculated. If the gel current values were close to those of their corresponding finite element models, it would indicate that the finite element modeling procedure produces correct values, validating it as an acceptable modeling protocol.

3.2 Circuitry Design

In order to produce a dual-frequency beat waveform, two BK Precision 3011B function generators at equal amplitude and at frequencies F_1 and F_2 respectively were used as inputs to a 0.65 gain summing amplifier circuit. The operational amplifier

used for the circuit was a 741 operational amplifier. The summing amplifier's output was connected to a 159 ohm resistor in series with the agar gel phantom, which was sandwiched between two stainless steel plates with resistivity of 0.72 micro-ohms*meter. The circuit was concluded by grounding the gel.

In order to perform measurements on the circuit, two Keithley 177 digital multimeters were placed across the output of the summing amplifier. The first was placed across both the 159 ohm resistor and the gel, while the second is placed across only the gel. The full circuit diagram is shown in figure 8.

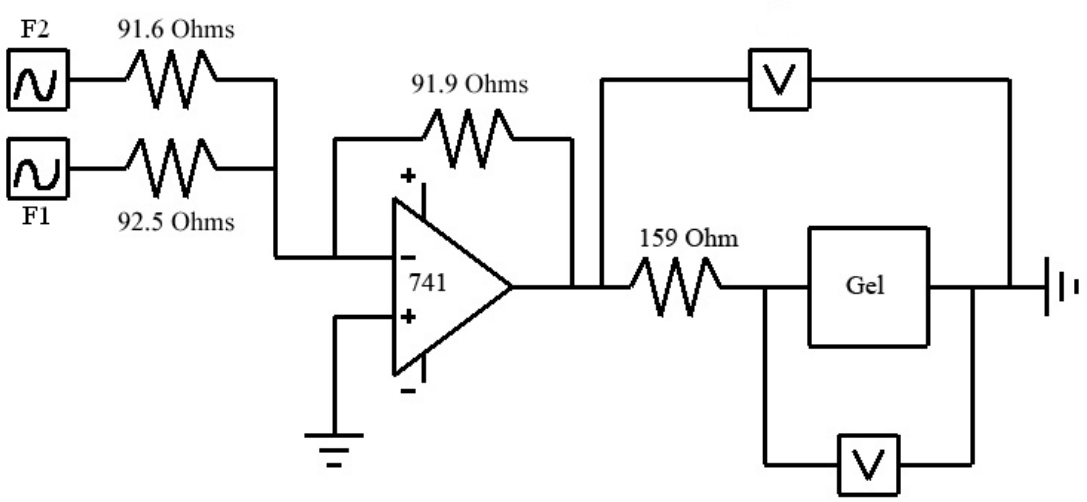

Figure 8 – Circuitry Diagram for Summing Amplifier and Gel

Three identical resistors were used for R1, R2, and Rf. The relative gain of each input was controlled by the ratio of Rf to its corresponding input resistor as shown in equation 8. The chosen resistors, in conjunction with the function generator output impedance of 50 ohms, resulted in a gain of 0.65 with both input currents equally weighted because of the identical resistors. Because of the applied alternating current, calculations of the output voltage required AC root mean square (RMS) values be used as noted in equation 9. The total output voltage from the summing

amplifier to the resistance system was 1.502 Vrms. Since an alternating current was used, the system was unaffected by sign changes as a result of the amplifier.

$$G_X = \frac{R_{91.9}}{R_X} \qquad (8)$$

$$V_{out} = R_{91.9} \cdot \left(\frac{V_{4000}}{R_{92.5} + R_{50}} + \frac{V_{4122}}{R_{91.6} + R_{50}} \right) \qquad (9)$$

3.3 Phantom Model Design

Each layer of the phantom model was comprised of 3.00 grams of agar and 75 milliliters of deionized water at 18.2 megaohm*m resistivity. Varying concentrations of sodium chloride were also used in order to vary the resistivity of the gel. In order to determine what resistivities could be created for the model, gels were produced with a range of salt concentrations as shown in table 3. The DI water was heated to a boil and then mixed with the agar and salt amounts shown in table 3. The mixture was stirred for three minutes while it cooled and solidified, followed by thirty minutes of additional cooling before it was ready for use. Once the gel was ready, it was taken from its glass petri dish, sandwiched between two stainless steel plates, and inserted into the circuit between the post-summation resistor and ground as shown in Figure 8. A full image of the gel and TENS circuit can be seen in Appendix 7.

Gel (mOsm)	*Agar (g)*	*Salt (g)*	*Water (mL)*	*Length (cm)*	*Width (cm)*	*Resistivity (Ω*m)*
0 (top)	3.00	0.00	75	8.75	1.5	15.508
0 (bottom)	3.00	0.00	75	8.75	1.5	16.663
145	3.00	0.32	75	8.75	1.5	4.857
290	3.00	0.64	75	8.75	1.5	2.936
435	3.00	0.96	75	8.75	1.5	2.044

Table 3 – Properties of Agar Gels

For the two and three-layer models, the gels were first tested individually to obtain single-layer results and then placed into the circuit in contact with each other to make the multiple layer models. The two two-layer phantom models used 135/435 milliosmole salt concentrations (0.32g, 0.96g) and 0/0 milliosmole salt concentrations (0.00 g). The three-tissue model used 0/290/0 milliosmole salt concentrations (0.00 g, 0.64 g, 0.00 g).

3.4 Model Calculations

In order to validate the ANSYS modeling method and determine if it was suitable for modeling the full electrical properties of a TENS device, the total current calculated in each finite element model was compared to the current measured in its corresponding phantom model. The resistivities described in table 3 were the same as those used in each ANSYS finite element model.

Total current, which was calculated by integration of the current density across the cross-sectional area of the cylindrical gel, was determined by equation 7. The total current values were compared to current measurements in the phantom models.

The electric field in the model was calculated in ANSYS on a node-by-node basis using equation 10. Vector directionality for the electric field was based on the direction of increase or decrease in potential. The current density was calculated using equation 11 and the solving method required the conductivity matrix shown in equation 12 (ANSYS Inc., 2007).

$$\{E\} = -\nabla V \qquad (10)$$

$$\{J\} = [\sigma]\{E\} \qquad (11)$$

$$\sigma = \begin{bmatrix} \frac{1}{\rho_{XX}} & 0 & 0 \\ 0 & \frac{1}{\rho_{YY}} & 0 \\ 0 & 0 & \frac{1}{\rho_{ZZ}} \end{bmatrix} \qquad (12)$$

3.5 Phantom Model Calculations

The current through the system was determined by equation 10, which allowed us to determine the resistance of the gel by Ohm's Law (equation 11, rearranged). The total voltage drop across the system (Vsys) was measured by the first multimeter, while the voltage drop across the gel (Vgel) was measured by the second. Once the resistances were determined, the resistivities of the gels were determined by equation 12, which normalized the resistances in relation to physical dimensions (Reilly, 1998). The resulting resistivities and the physical dimensions of the gels are listed in table 3. The gel resistivities were placed into the ANSYS simulations described in chapter 2 in order to validate the finite element models against experimental data.

$$I = \frac{V_{sys} - V_{gel}}{159\Omega} \qquad (10)$$

$$R_{gel} = \frac{V_{gel}}{I} \qquad (11)$$

$$\rho_{gel} = R \cdot \frac{\pi \cdot r^2}{l} \qquad (12)$$

3.6 Single Component Model Validation

The total current in each finite element model was calculated as shown in equation 7, and the final calculations are shown in table 4. In order to adjust the calculations on a two dimensional model to a three dimensional gel, the 2D model was

treated as a 2D gel and the current density was multiplied by the full area of the gel instead of just along the length of the rectangle. The simulated currents were compared to experimental currents, which were calculated using equation 10.

Gel (mOsm)	*Vsys*	*Vgel*	*Simulated Current (A)*	*Experimental Current (A)*	*Difference (%)*
0	0.5238	0.1025	0.00265	0.00265	0%
0	0.5221	0.1082	0.00260	0.00260	0%
145	0.5276	0.0128	0.0320	0.00324	1.25%
290	0.5020	0.0221	0.00302	0.00302	0%
435	0.5294	0.0075	0.00324	0.00328	1.22%

Table 4 – Voltage and Current Values for Simulated and Experimental Gels

The simulated current calculations were very close to the experimental values. Agar was sufficient in order to validate that ANSYS was producing correct quantitative values for single-layer models. However, due to experimental abnormalities it appeared that agar cannot be used to validate the ANSYS models for multi-tissue systems.

3.7 Model Abnormalities

There was some concern that using agar gel as the phantom model might cause difficulties due to its inherently aqueous nature and the possibility of mixing between gel layers. This would alter the resistivity values and decrease the phantom model's accuracy. Performing voltage measurements across the three-tissue simplified model (0/290/0) at initial insertion into the circuit and again fifteen minutes later confirmed that the electrical properties of the gel were changing over time. The resistivity of the gel components went from 15.51, 0.28, and 16.66 Ω*m respectively to 9.74, 0.72, and 5.40 Ω*m. These values are noted in table 5.

It is important to note that the gel least affected over time was the first 0 milliosmole gel, which was also the topmost gel in the circuit. In addition to ion leaching as a result of the alternating current and generic diffusion, gravitationally

Gel (mOsm)	*Agar (g)*	*Salt (g)*	*Water (mL)*	*Length (cm)*	*Width (cm)*	*Resistivity (Ω*m)*
0 (top)	3.00	0.00	75	8.75	1.5	9.737
0 (bottom)	3.00	0.00	75	8.75	1.5	5.400
290	3.00	0.64	75	8.75	1.5	0.718

Table 5 – Gel Resistivities Post-Leaching

forced mixing of the middle and bottom gel played a role in the resistivity change over time.

In order to determine if the gels were exhibiting ion leaching, the 135/435 gels were placed into the circuit again. Additionally, a set of 0/0 gels was created in order to see if there was any resistivity change between identical concentrations. On insertion into the circuit, the 135/435 two-layer model showed a similar change in properties to the 0/290/0, but there was no alteration in properties for the 0/0 gels when placed into the circuit. As a result, it was concluded that agar based models are not suitable phantoms for a multi-unit electrical property model due to the presence of ion leaching between gels of different ionic concentrations. Future work will be necessary in order to determine a suitable phantom model for multi-part electrical simulations. It is possible that a gel-based substance may work if some form of barrier can be placed between each layer that is conductive but prevents leaching such as additional metal plates. Early attempts at correcting the leaching problem were performed using steel plates of resistivity 0.72 microohms*meters. This was successful in maintaining gel properties, but resulted in other modeling problems. The gel models no longer acted like they were in series when the steel plates were introduced into the system, possibly due to the creation of multi-layer capacitors.

CHAPTER 4

FULL SIMULATION MODEL

4.1 Model Design

Because the ANSYS simulations were able to be validated for single-tissue simplified models, a higher complexity model was generated in order to better model the electrical properties resulting from use of a TENS device *in vivo.* An image of the upper arm of a human male was chosen from the Visible Human Project as the point of application for the TENS device. This arm segment is shown in figure 9. (Visible Human Project, 2006.)

Figure 9 – Visible Human Arm Image

First, the arm image was isolated from the body image by use of Adobe Photoshop 8.0, and then Scion image processing software was used in order to convert the arm image into an edge drawing. Interior details were sharpened as necessary in Photoshop in order to maintain contrast between tissue layers. The resulting edge drawing is shown in figure 10.

The edge drawing was imported into Photoshop at 33% transparency, and the line tool was used in order to trace the structure of the arm. Only straight lines were used, which resulted in curves being approximated by a discrete number of lines. This was done in order to simplify the meshing procedure for the model and shorten the

calculation time, as calculations take an exponentially increasing amount of time in proportion to model complexity. As can be noted in a comparison between figures 10 and 11, the structure was also simplified during the tracing procedure. This was also done for the purpose of decreasing calculation times. The completed line drawing was then placed into a 10 screen-pixel grid, the origin defined in the bottom left corner of the image, and saved. The results of this are shown in figure 11.

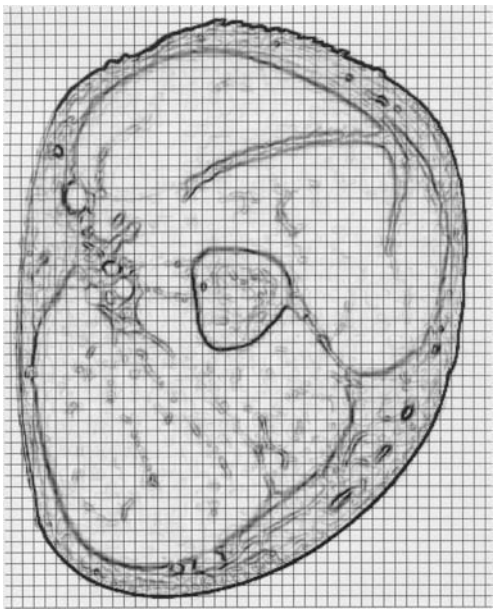

Figure 10 – Edge Drawing

From here, each intersection point of a line was marked by coordinates in relation to the assigned origin of the image. The 372 points in the image were assigned as keypoints in ANSYS during the model building process. Each keypoint was sequentially entered into the model by coordinates relative to the origin. The model consists of 372 keypoints, 381 lines, 55 areas, and 7,415 nodes. A highly refined mesh was not used at this stage because of exponentially increasing calculation times.

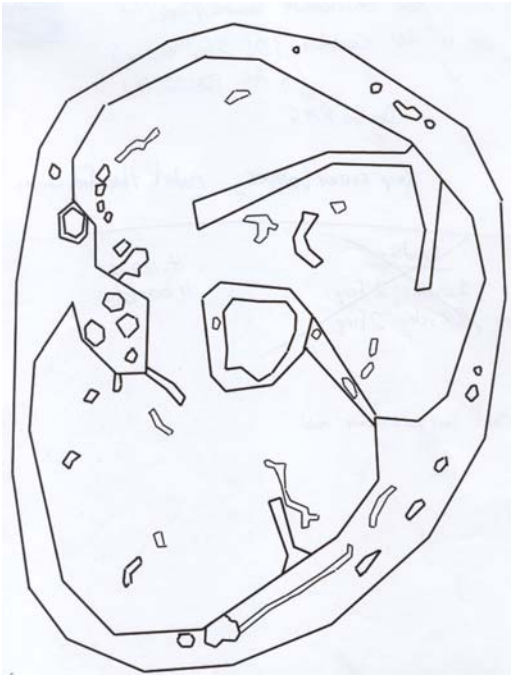

Figure 11 – Arm Lines

4.2 ANSYS Model Development

The intersection points noted in section 4.1 were taken and entered into ANSYS as a series of keypoints. This keypoint field is the basis of the model, and all the geometry in the development of the arm model was based on them. The full keypoint matrix is shown in figure 12. The traced lines from which the keypoints were generated were recreated by connecting all of the keypoints to the appropriate neighboring points. The *Create Line by Keypoints* tool in ANSYS was used in order to manually build the lines, and the resulting line image is shown in figure 13.

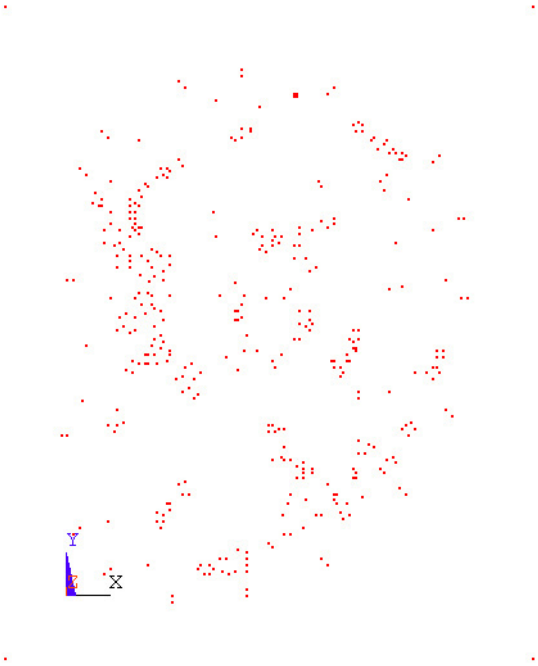

Figure 12 - Keypoint image

The lines were used as boundaries for the designation of areas. Areas were indicative of the different tissues which would be found in the human body. As was the case with the simplified models in chapter 2, each type of tissue was assumed to be homogeneous in space and identical in properties to other tissues of the same type. As an example of the results of these assumptions, the properties of skin were applied to all areas designated as skin, across all eventual nodes meshed within that area.

Defining areas by line boundaries filled the entire area encompassed by those lines. At this point in development, the outer skin layer incorporated everything in the model, while the muscle layer incorporated all the internal fat and bone segments as well. In order to make the model function properly, the inner areas were subtracted from the outer areas using the boolean *ASBA* command in ANSYS to make each tissue

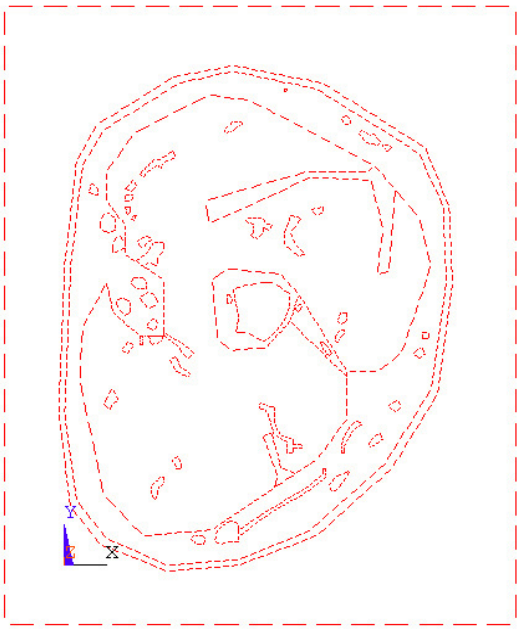

Figure 13 – Line Image

a separate unit. Once subtracted, the areas were glued together using the *GLUE* command. This connected all the borders so that conductive transfer occurred and the tissues were not treated as perfectly insulated. The model shown in figure 14 now consisted of multiple tissues connected together into one large arm unit.

In order to define the properties of the tissues within the model, electrical properties designating the permittivity and resistivity were applied to each tissue type. These values are defined in tables 1 and 2. Skin, fat, muscle, nerve, connective tissue, blood, cancellous and cortical bone were chosen as the materials. These were each defined as a subtype of the PLANE223 Quad 8-node element, which is the ANSYS designated element type for coupled field analysis. Once these values were applied to

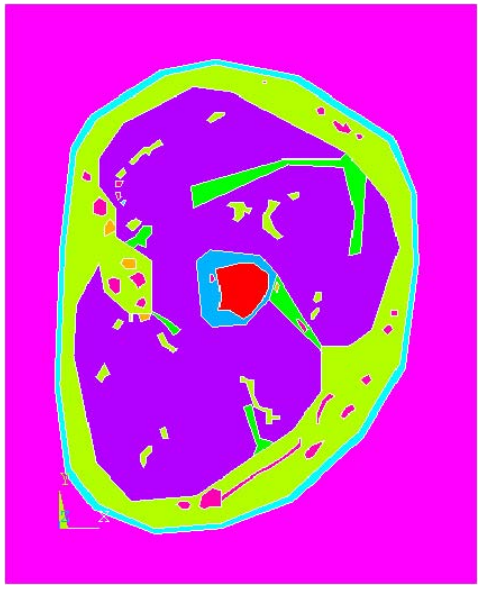

Figure 14 – Area Image

the appropriate tissues, the model was meshed in order to prepare it for calculations. The meshing procedure assigned each material to its appropriate areas and discretized each area into calculation points (nodes). The meshed structure of the model is shown in figure 15.

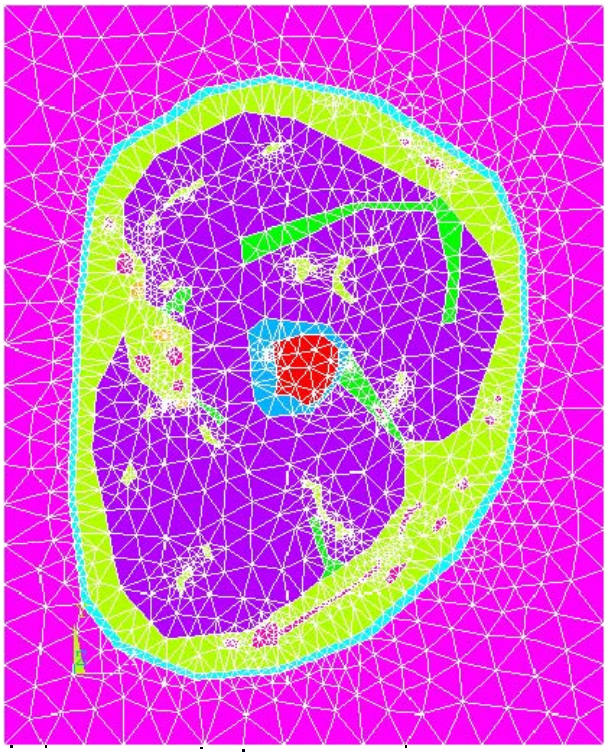

Figure 15 – Meshed Image

4.3 Model Loading and Calculations

Due to the nature of the ANSYS software, it was not possible to create two different frequencies of alternating current in the same model. In order to circumvent this restriction, voltages were determined in MatLab based on the desired current frequencies shown in Appendix 1. Each voltage determined in MatLab was entered as a separate load step in the ANSYS model. Due to the time-intensive nature of entering the load steps individually, this model resulted in a low sampling resolution 160 time-step model over the 8 milliseconds of oscillation in each cycle. Quantitative analysis was then performed by ANSYS to determine the electric potential, field, and

current density for each load point in sequence. These results were then linked in order and animated to view over time, which allowed for monitoring electrical properties of the arm in response to the alternating current applied. The potential, electric field and current distribution at time t=0.008 seconds are shown in appendices 4-6 respectively.

The electric potential through the arm showed a large drop across the skin layer. This makes sense qualitatively, as the skin had the highest resistivity in the model. As a result of this potential drop, the electric field was greatest across the skin layer as well, and it was very low throughout the rest of the arm in comparison.

The current density in the arm showed the preferred current path through the arm to be through connective tissue when possible and through muscle otherwise. Very little current passed through fat layers other than those directly in the path of the electrodes. Cortical bone also showed very low current passing through it. The current distribution seems feasible because the paths taken by the current correspond to materials with higher conductivities.

4.4 Conclusions

It was concluded, as a result of this project, that the model creation method demonstrated in chapter 4 was an effective means of creating complex two-dimensional finite element models in ANSYS to simulate electrical conditions in human body segments. It was also determined that ANSYS is a suitable finite element modeling program for simulation of single material models. While ANSYS was able to produce multi-layer models, due to abnormalities in experimental measurements it was unable to be validated as a multi-layer simulation program. Ion leaching between gel layers resulted in changes over time of electrical properties of the phantom models. This prevented comparison of ANSYS simulation results to experimental

measurements and calculations.

Agar gel was determined to be a suitable material for single-layer and single-material multi-layer phantom models. Due to ion leaching between gel layers of different salt concentrations, it was not suitable for use as a multi-material phantom model.

4.5 Future Work and Improvements

There are several areas where this project can be improved on in the future, both in the simulation and the experimental phantom sections. The primary concern to be addressed is the inability to create a functional multi-tissue gel phantom because of ionic leaching between gels. Either a recreation of the phantom models with a more stable, likely non-aqueous phantom structure or some means of preventing leaching between gel layers, such as metal plates between each layer, will be required in order to make the phantom structure work for more complex models. Because of the complex internal structures of the arm simulation, it is possible that an entirely different phantom modeling procedure may be needed.

If the gel leaching problem is solved, attempts could be made at altering the electrode placement to the radial edges of the gel instead of the cross-sectional edges. Gels of different resistivities could then be placed into the main gel in order to simulate internal structures. Alternatively, the phantom model could be replaced with a circumferential slice from a bovine or porcine leg. These would more closely mimic the conditions found in a human arm.

The resolution of the ANSYS arm model was too low for accurate calculations. As Appendix 3 shows in comparison to Appendix 1, the 160 time step voltage model suffers from attenuation sampling error on the F_2 current. This limited the effectiveness of the model. Due to the time-constraints of determining the voltage

pairs and entering them into load steps by hand, it would be advisable to write MatLab code to generate an ANSYS script. ANSYS scripting allows one to import a text file containing a list of commands to perform on a pre-existing model, and MatLab code can generate text files. If a program was written in MatLab which generated an output text file which was formatted to match ANSYS scripting conventions, it would be possible to have it generate the script needed to automate the entry of large numbers of load steps. Assuming calculation time for ANSYS analysis of the load steps does not become prohibitively long on the addition of more load steps, this would solve the resolution problem.

APPENDIX 1 – Waveforms for F_1 and F_2 Hz Alternating Currents

The blue line designates the F_2 current.

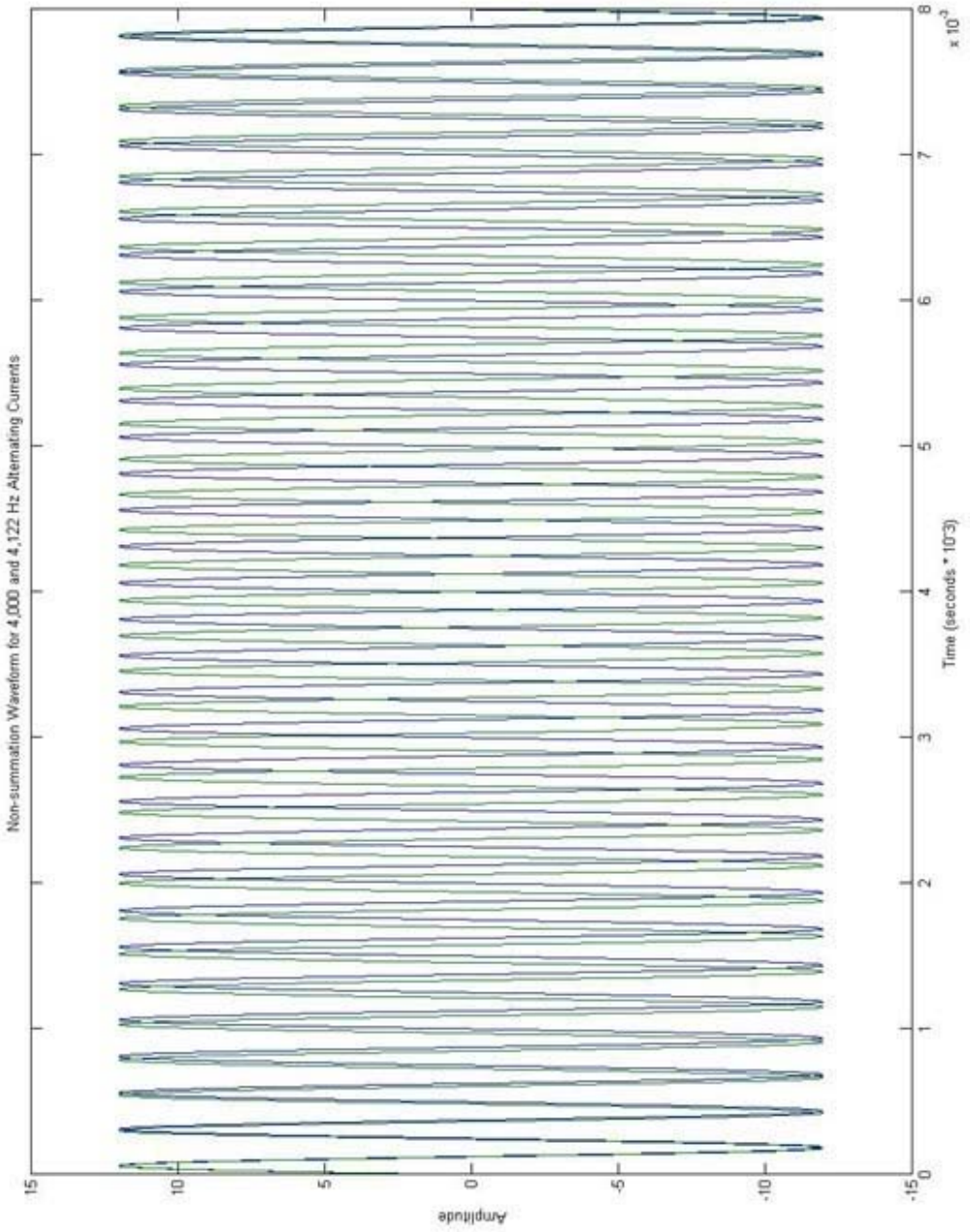

APPENDIX 2 – Summation Waveform for $F_1$and F_2 Hz Alternating Currents

This represents a single dF cycle for the Biowave TENS device.

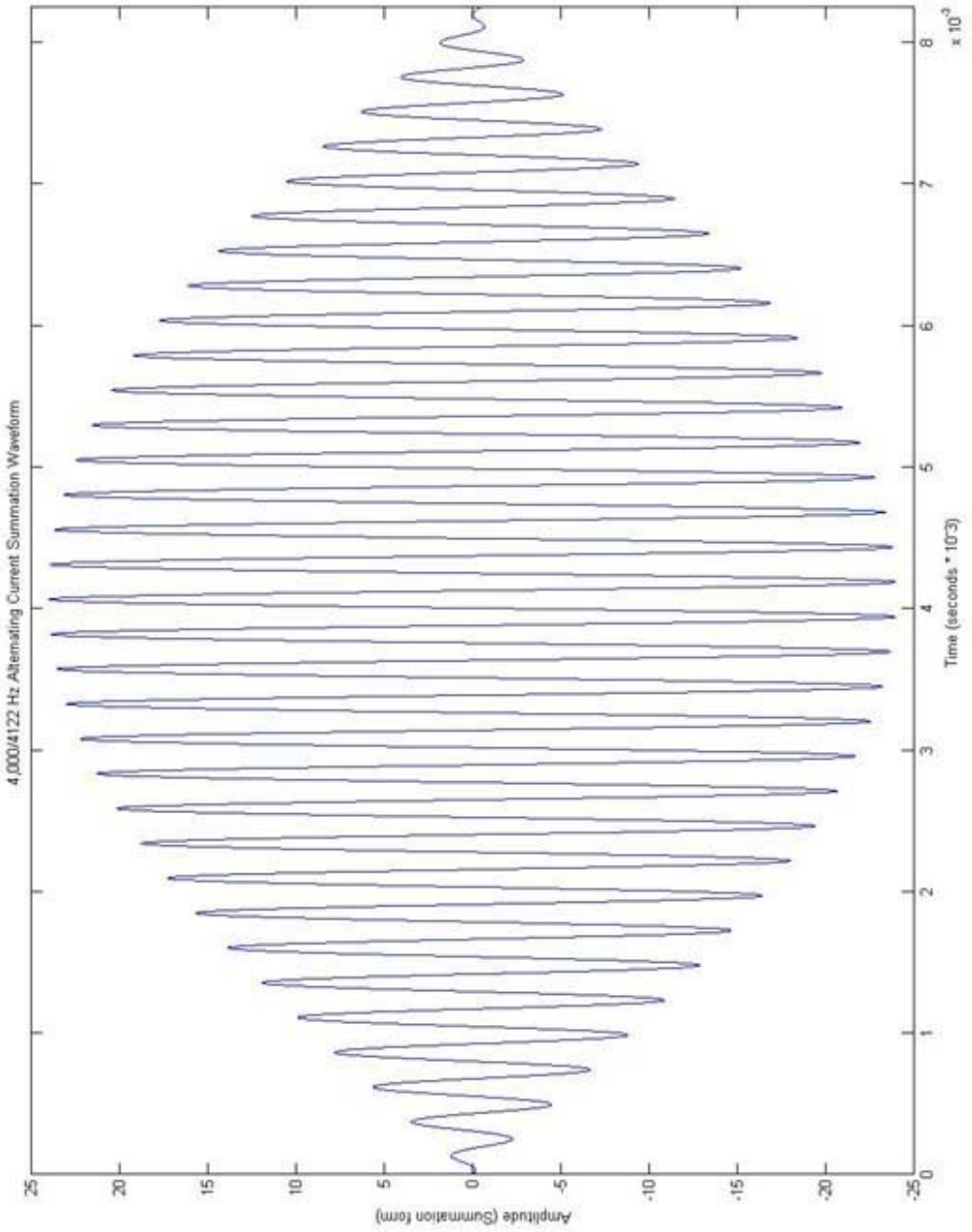

APPENDIX 3 – Attenuation Errors in 160 Time-Step Voltage Model

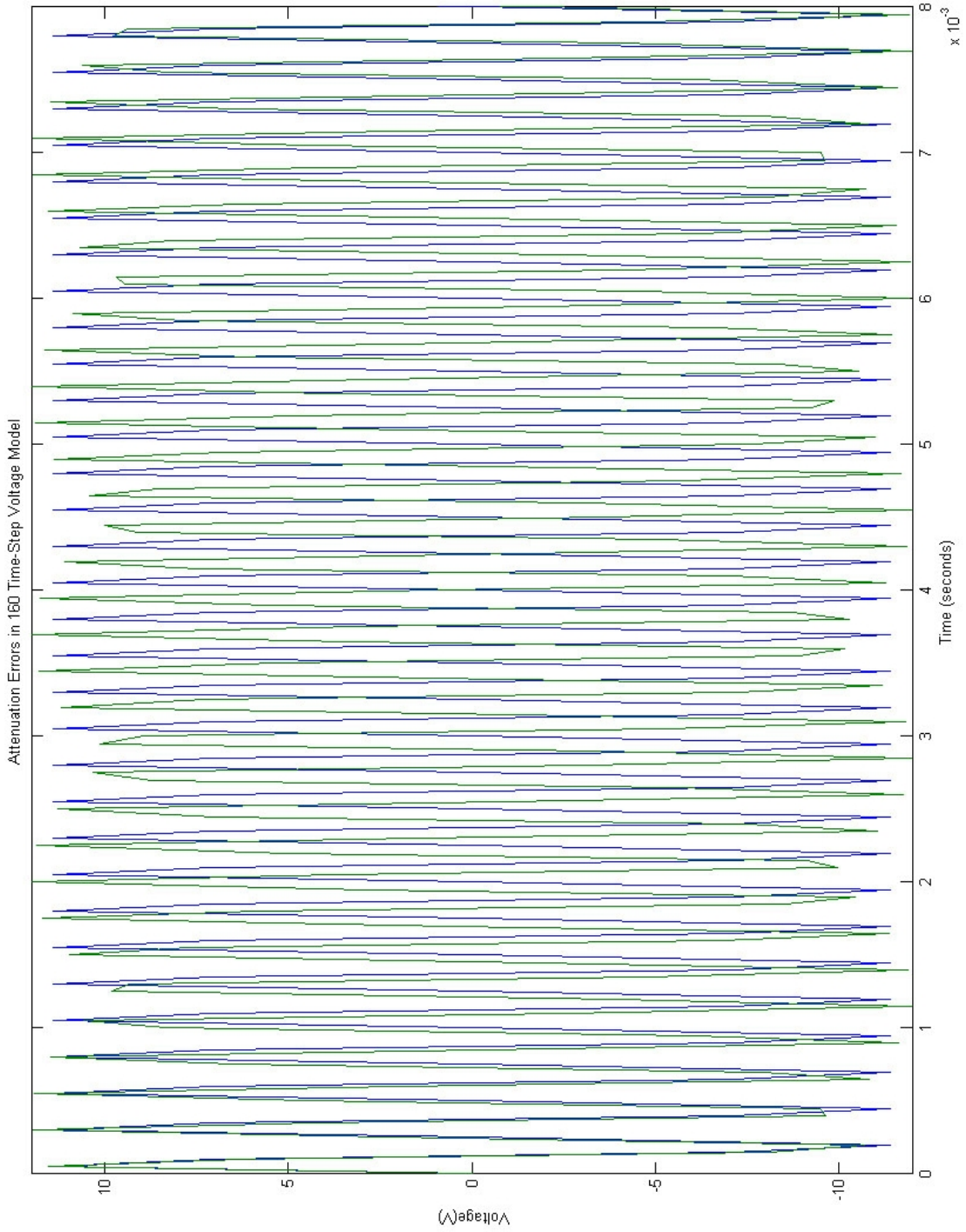

APPENDIX 4 – Electric Potential in Arm Model at 0.008 seconds

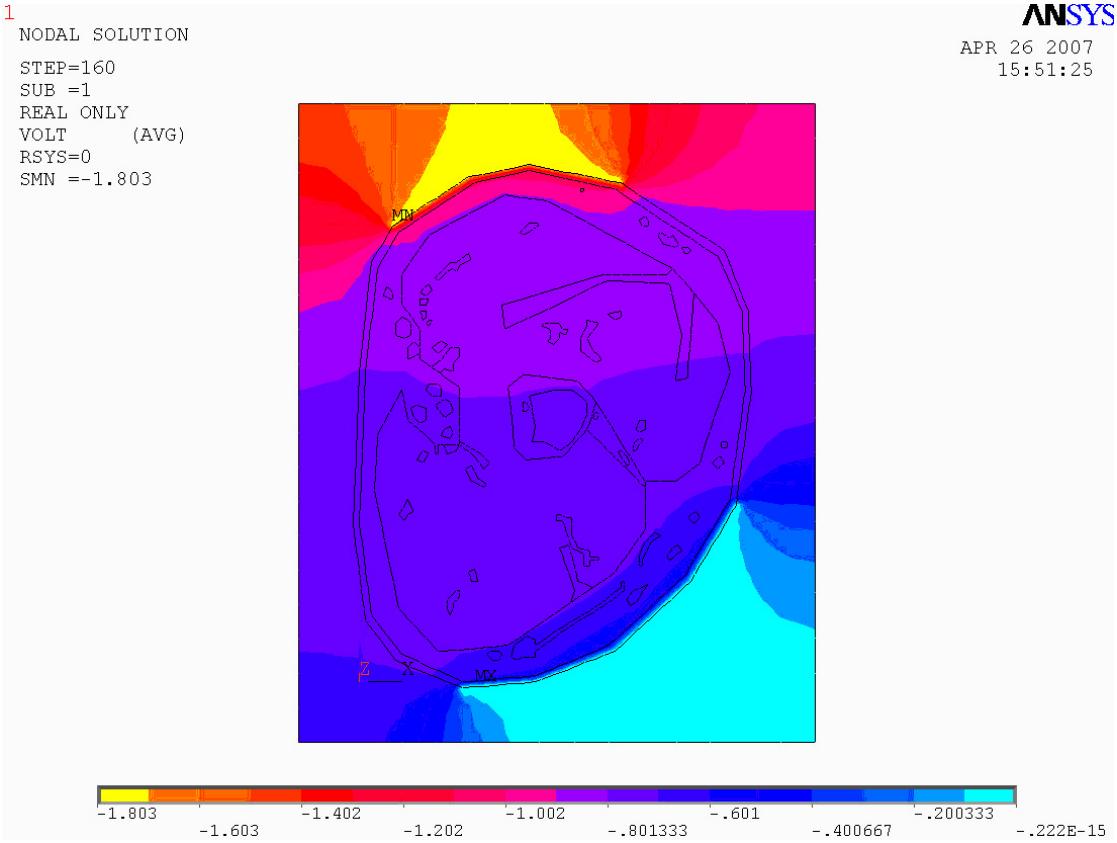

APPENDIX 5 – Electric Field in Arm Model at 0.008 seconds

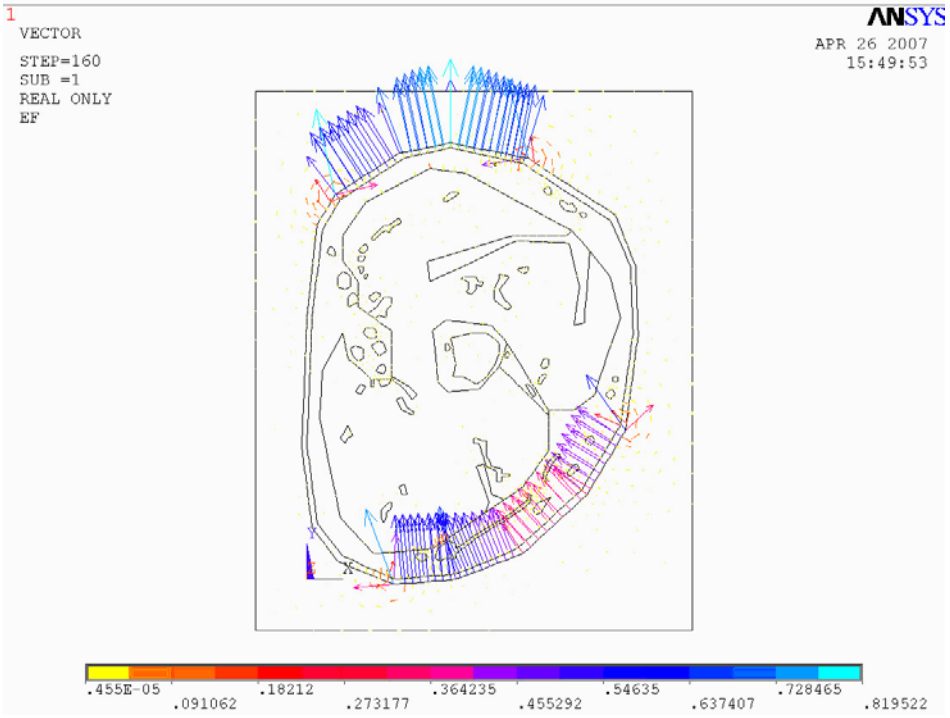

Electric Field in Arm Model – Vector Image

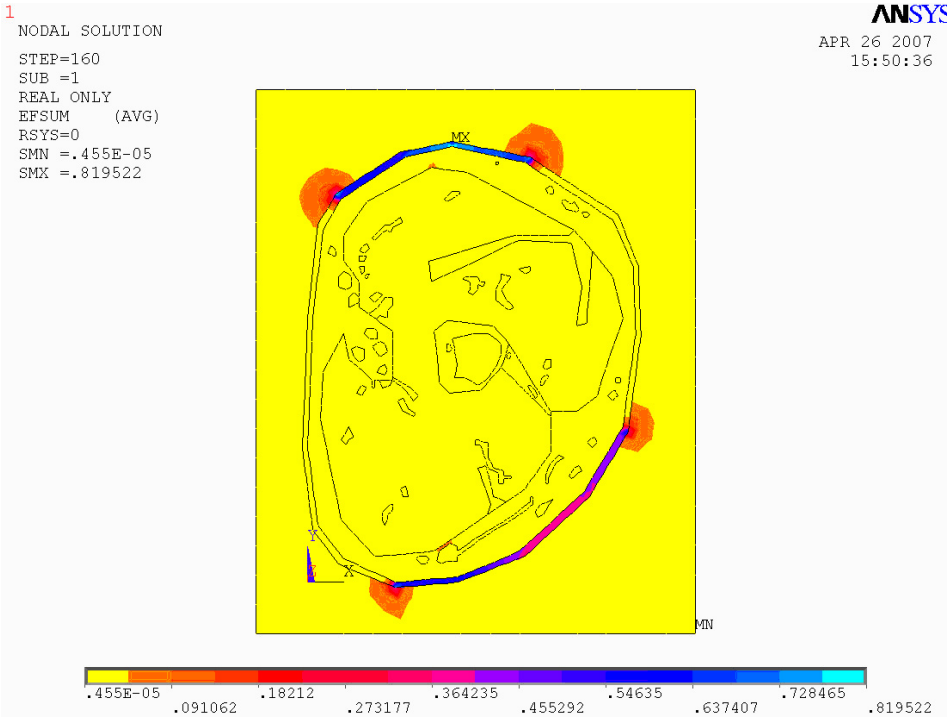

Electric Field in Arm Model – Contour Image

APPENDIX 6 – Current Density in Arm Model at 0.008 seconds

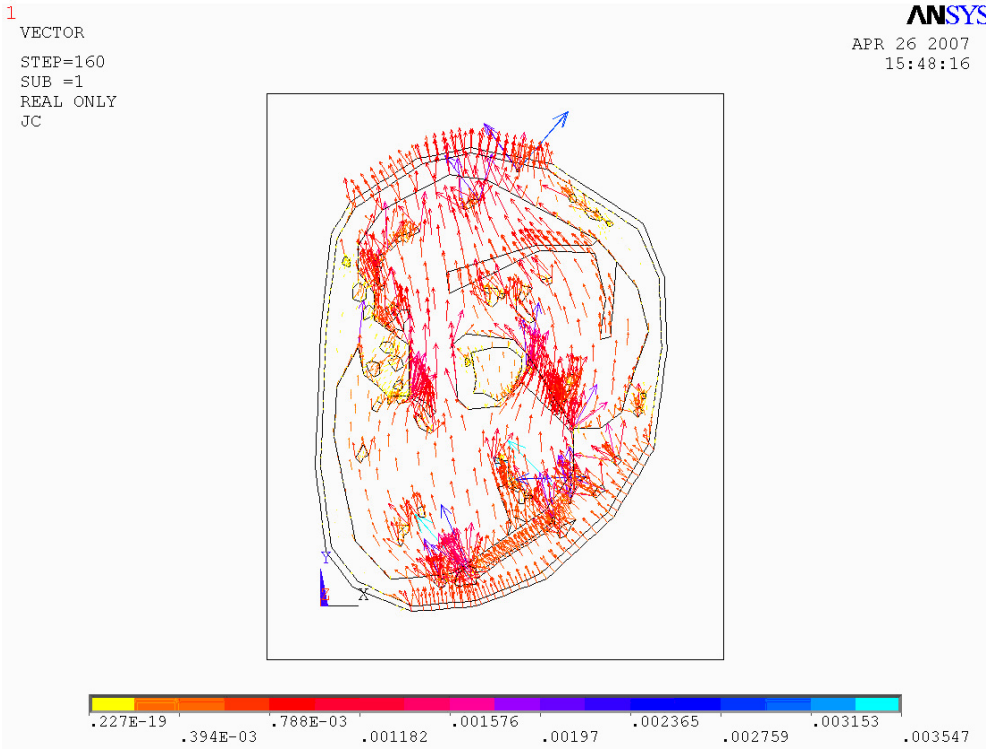

Current Density in Arm Model – Vector Image

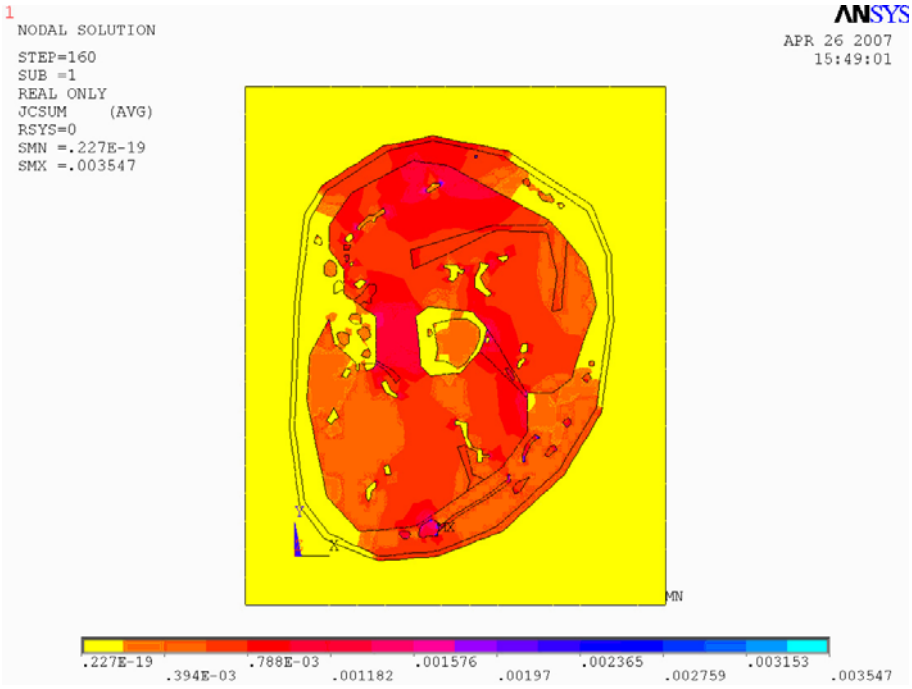

Current Density in Arm Model – Contour Image

APPENDIX 7 – TENS Circuit and Gel Connection

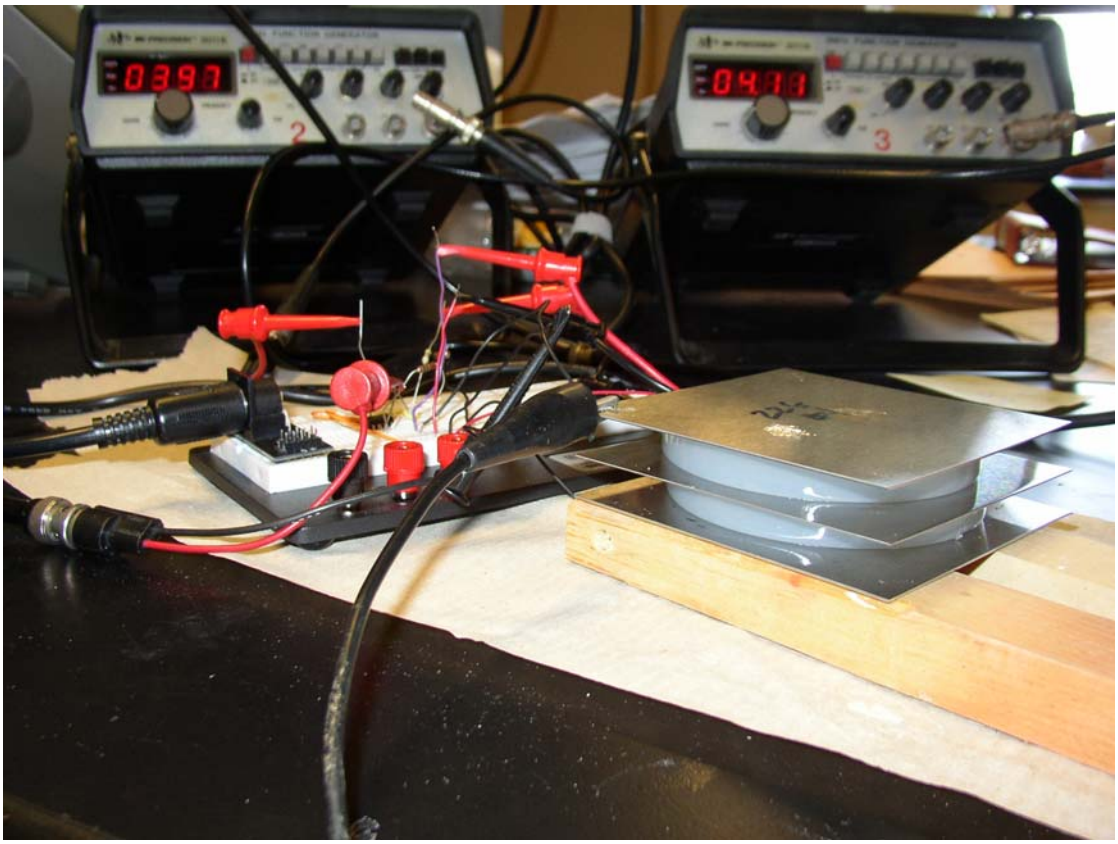

This is the TENS circuit with the gels attached. This particular arrangement is measuring the voltage drop across the 145/435 mOsm gel arrangement. The added steel plate separating the gels is an attempt at preventing ion leaching.

APPENDIX 8 – TENS Circuit

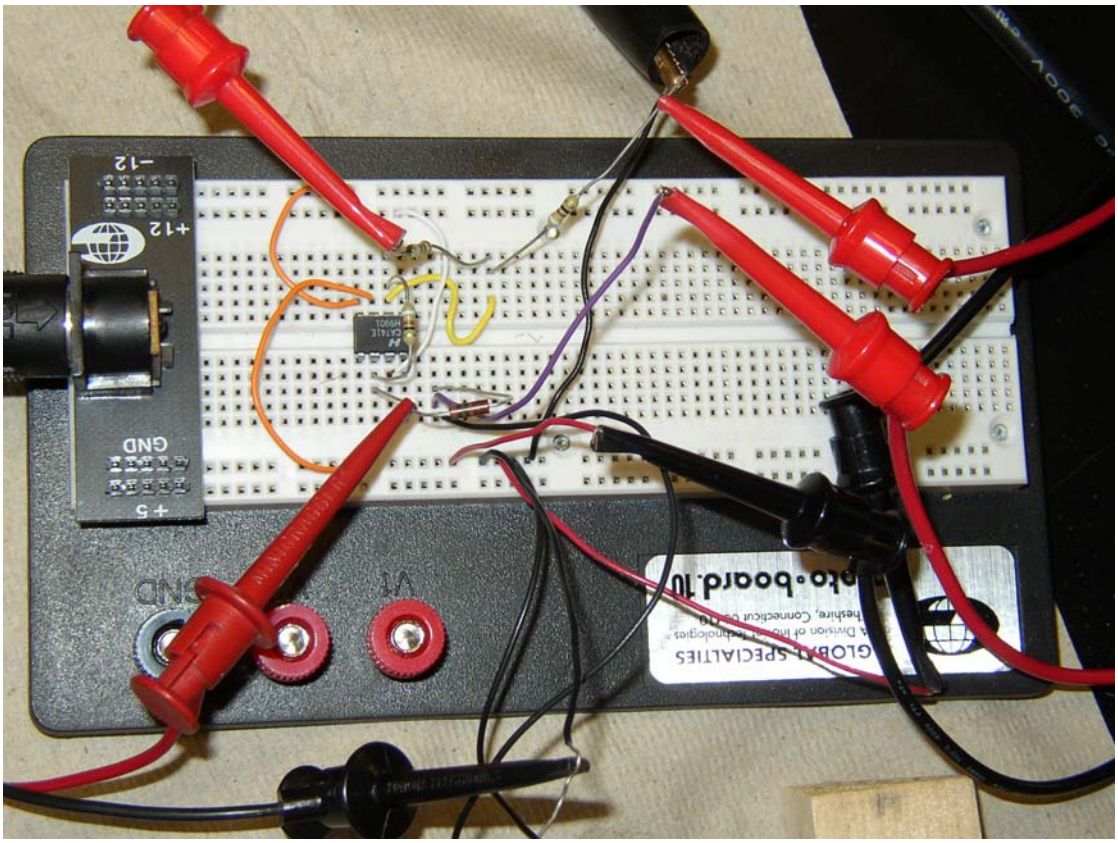

A non-schematic view of the TENS circuit.

REFERENCES

Reilly, J. Applied Bioelectricity: From Electrical Stimulation to Electropathology. Springer-Verlag Publications, New York. 1998.

Zhu F., Leonard E., Levin N. Body Composition Modeling in the Calf Using Equivalent Circuit Model of Multi-Frequency Bioimpedance Analysis. Physiological Measurement. 26:133-143, 2005.

Yokoyama M., Morita K. et al. Comparison of Percutaneous Electrical Nerve Stimulation with Transcutaneous Electrical Nerve Stimulation for Long-Term Pain Relief in Patients with Chronic Low Back Pain. Anesthesiology and Analgesics. 98:1552-1556, 2004.

Gabriel, C. Compilation of the Dielectric Properties of Body Tissues at RF and Microwave Frequencies. Report, Occupational and Environmental Health Directorate. Radiofrequency Radiation Division, Brooks Air Force Base. 1996. (Report mirrored at http://niremf.ifac.cnr.it/tissprop/)

Katz S., Zlochiver S., Abboud S. Induced Current Bio-impedance Technique for Monitoring Bone Mineral Density – A Simulation Model. Annals of Biomedical Engineering. 34(8):1332-1342, 2006.

Babineau D., Longtin A., Lewis J. Modeling the Electric Field of Weakly Electric Fish. Journal of Experimental Biology. 209:3636-3651, 2006.

Melzack R, Wall P. Pain mechanisms: a new theory. Science. 150(699):971-979, 1965

Hamza, M., White P., et. al. Percutaneous Electrical Nerve Stimulation: A novel analgesic therapy for diabetic neuropathic pain. Diabetes Care. 23(3):365-370, 2000.

Cummings, M. Percutaneous Electrical Nerve Stimulation – Electroacupuncture by Another Name? Acupuncture in Medicine. 19(1):32-35, 2001.

Cooperberg M., Stoller M. Percutaneous Neuromodulation. Urologic Clinics of North America. 32:71-78, 2005.

Manola L., Holsheimer J., Veltink P. Technical Performance of Percutaneous Leads for Spinal Cord Stimulation. Neuromodulation. 8(2):88-99, 2005.

ANSYS Theory Manual. ANSYS, Inc. Included with ANSYS software packages. http://www.ansys.com 2007.

Transcutaneous Electrical Nerve Stimulation: WebMD eMedicine. http://www.emedicine.com/pmr/topic206.htm January 26, 2007

The Visible Human Project. National Library of Medicine. 2006 http://www.nlm.nih.gov/research/visible/visible_human.html